IEEE Access
Multidisciplinary | Rapid Review | Open Access Journal

Received September 6, 2021, accepted September 17, 2021, date of publication September 20, 2021,
date of current version September 28, 2021.

Digital Object Identifier 10.1109/ACCESS.2021.3114216

Exploring the Utilization of Energy Storage Systems for Frequency Response Adequacy of a Low Inertia Power Grid

MD. NAHID HAQUE SHAZON[1], (Graduate Student Member, IEEE), NAHID-AL-MASOOD[1], (Senior Member, IEEE), HASIN MUSSAYAB AHMED[1], SHOHANA RAHMAN DEEBA[2], (Member, IEEE), AND EKLAS HOSSAIN[3], (Senior Member, IEEE)

[1]Department of Electrical and Electronic Engineering, Bangladesh University of Engineering and Technology, Dhaka 1205, Bangladesh
[2]Department of Electrical and Computer Engineering, North South University, Dhaka 1229, Bangladesh
[3]Department of Electrical Engineering and Renewable Energy, Oregon Renewable Energy Center (OREC), Oregon Tech, Klamath Falls, OR 97601, USA

Corresponding author: Nahid-Al-Masood (nahid@eee.buet.ac.bd)

ABSTRACT The utilization of Energy Storage Systems (ESS) for improving the frequency response of a low inertia power system is investigated in this article. Substantial wind power penetration is causing the replacement of conventional synchronous generators in several power systems. Variable speed wind machines traditionally do not contribute to frequency regulation without additional control strategy. As a result, a wind dominated power grid may have inadequate inertia and governor responsive reserve. In such situation, a large contingency may yield undesirable Rate of Change of Frequency (ROCOF) and frequency deviation. To overcome this problem, deployment of ESS, namely, Superconducting Magnetic Energy Storage (SMES) and Battery Energy Storage System (BESS) can be a worthwhile solution. Since these devices are costly, their appropriate sizing and operational approach are crucial. Therefore, in this paper, analytical expressions are derived to find the minimum ratings of SMES and BESS. To this end, system frequency deviation, ROCOF, inertial response and governor response are taken into account. Also, a coordinated operational strategy is proposed to retain frequency response adequacy and minimize under-frequency load shedding where SMES is triggered when system ROCOF supersedes a certain limit and BESS is activated due to system frequency surpassing a preset threshold. The performance of the proposed strategy is explored in a low inertia network under substantial wind penetration considering several different wind penetration levels. Also, the results are validated against two existing approaches. Simulation results reveal that the proposed methodology considerably enhances the frequency response in various operating conditions.

INDEX TERMS Energy storage systems, low inertia power system, frequency response, under-frequency load shedding.

I. INTRODUCTION

In recent times, traditional synchronous generators are being decommissioned in many power systems. The primary driving forces behind this trend are depletion of reserve and negative impact of fossil fuels on the environment. Among possible alternatives, wind energy is considered to be one of the most convenient options [1]. However, increased integration of wind power plants introduces further challenges regarding the frequency response adequacy, especially in a low inertia power system. This is because nowadays wind power plants predominantly utilize type III (Doubly Fed Induction Generator: DFIG) and type IV (Full-Scale Converter: FSC) machines. These variable speed machines are isolated from the grid through power electronic converters [2]. Therefore, they generally do not provide inertia and governor response (also known as primary frequency response) unless additional control strategy is implemented [3]. As such, frequency response after a major contingency is likely to become more vulnerable under high wind power penetration [4]. Situations can arise where a

The associate editor coordinating the review of this manuscript and approving it for publication was Lin Zhang.

system has substantial wind penetration while it imports bulk amount of power through high voltage AC (HVAC) interconnection from adjacent grid. In such a condition, only a few synchronous generators can be present in the power importing zone. During this situation, a large contingency (e.g. tripping of an interconnection) may cause unacceptable frequency excursion with a high Rate of Change of Frequency (ROCOF) and frequency deviation. Consequently, significant Underfrequency Load Shedding (UFLS) may need to be applied to arrest the frequency decline.

Note that when ROCOF exceeds 2 Hz/s, steam, hydro and wind turbine generators face difficulties to be in synchronism [5]. Furthermore, if ROCOF is higher than 3 Hz/s, the UFLS relays may fail to respond quickly enough to shed necessary amount of loads. It eventually could result in a system wide blackout [6]. Furthermore, while shedding loads, distributed generators can also get disconnected [7]. Such incident makes frequency response even worse, which ultimately leads to further load shedding. Therefore, necessary techniques need to be adopted to avoid high ROCOF and large frequency deviation to improve the frequency resilience.

Various strategies are explored in the existing literature to improve the frequency response of low inertia grids. For example, utilization of synchronous condensers is reported in [8], which can provide supplementary inertial response. Further, synchronous condenser and synthetic inertia from wind plants are jointly used in [9] to enhance frequency stability. Note that in both of these works, the ratings of synchronous condensers are chosen based on corresponding simulated grid topology. Thus, no analytical methodology is developed to find the optimal size of additional frequency support device (i.e. synchronous condensers).

A methodology is developed in [10] to incorporate virtual inertia support from wind plants into generation scheduling by utilizing the DC-link inertia control, the VCC strategy and power-frequency droop control. However, neither competency of the proposed methodology is compared with any existing technology nor value proposition of the proposed methodology is illustrated in this work. Furthermore, various storage technologies are utilized for achieving fast frequency response [11]. Among them, Li-ion batteries are widely used as storage medium. Alternative lithium batteries [12], Ni-Cd, lead-acid, vanadium redox flow batteries, flywheels [13], supercapacitors [14] and Superconducting Magnetic Energy Storage (SMES) [15] are also employed for frequency support. Their response time, installation cost, operational cost, sustainability and life spans are described in [16]. However, none of these illustrated works emphasis on finding appropriate sizing of the aforementioned energy storages and their economic feasibility. For instance, in [14], the authors only demonstrate the competency of ultracapacitor installation under different load condition. Furthermore, effectiveness of supercapacitor installation is not compared with any existing technologies such as synchronous condenser, BESS, SMES and so on. In [17], ultracapacitor storage is used as a Dynamic Energy Storage System (DESS) to offer emulated inertial support. Nevertheless, the authors primarily focus on structure and control of the DESS instead of its sizing. In [18], an optimally sized Battery Energy Storage System (BESS) is incorporated to provide primary frequency response, where BESS size is determined solely based on economic aspect without taking frequency response adequacy in different conditions into account.

In [19], a bi-level optimization model is developed for achieving maximum profit where the model is converted into a mixed-integer linear program. According to this algorithm, the optimal size of the energy storage depends on system fault condition, duration of load curtailment under various fault scenarios and enhancement of profitability in terms of unit income for distribution system. However, system resilience is neither investigated under altering renewable penetration level nor system operating conditions such as frequency and ROCOF are taken into account.

In [20], authors propose a sizing scheme for energy storage systems to mitigate significant changes in power outputs of intermittent sources. The authors consider generator ramp-rate limits, the efficacy of storage system (State of Charge limits) and optimal dispatch of the energy storage systems along with curtailment of intermittent resources. The primary objective of this work is to obtain an optimal energy storage size so that minimum curtailment of renewable sources is achieved. Nevertheless, the sizing strategy does not take any other system operating conditions into consideration and implementation of this algorithm does not depend on any system parameters. In addition, there is no indication that which storage device would be preferable to obtain maximum profitability.

The authors propose a sizing scheme for Battery Energy Storages, which solely depends on optimizing operational cost of a microgrid and minimizing BESS charging and discharging capacity in [21]. This research work investigates the competence of the proposed method in three different scenarios depending on whether the microgrid is connected with the host grid and power can be sold to the host grid. Thus, system performance is not examined in terms of allowable frequency deviation and system ROCOF limits.

In [22], authors incorporated a multi-objective grey wolf optimizer to determine optimal Hybrid Energy Storage System size considering system operating cost and battery lifespan. Competency of the methodology has been scrutinized by comparing the obtained total energy loss with that of RF based Energy Management System. In [23], authors propose a sizing methodology of ESS to determine ESS rated power and energy capacity for providing inertial and primary frequency support by utilizing linearized swing equation.

From the above literature review, the limitations of these research works are summarized below.

- A number of existing works do not concurrently consider frequency deviation, system ROCOF, inertial response and governor response for determining the ratings and competency of ESS.

- Over-dependency on time-domain simulations and optimization algorithms is noticed, which consider only profit maximization and battery state of charge to determine ESS sizes.
- Linearization of swing equation is done in many existing works to find optimal ratings of ESS. Consequently, the dynamic attributes of frequency excursion is not fully captured.
- Limited analyses of value proposition of ESS considering their installation, operation and maintenance costs are reported.

Lately, SMES has attracted the attention of researchers for its enormous charge/discharge cycles, rapid response time and high peak current handling capabilities [24]. Generally, SMES is utilized for providing short time storage support. In contrast, BESS is usually installed to deliver storage support for longer period. Consequently, combination of SMES and BESS is taken into account in various applications. These include compensating load variations in railway systems [25], mitigation of wind intermittency [24], electric vehicle operation [26] and so on.

It is evident that SMES can be used for providing additional inertial response to limit ROCOF. In addition, BESS can be used for offering inertia support as well as primary frequency response (i.e. akin to governor response) to arrest the frequency excursion above a certain threshold. Therefore, a combination of SMES and BESS can be beneficial to reinforce the frequency resilience of a low inertia grid. However, coordinated action of SMES and BESS to improve frequency response of renewables dominated power systems remains unresolved in the recent literature. Note that SMES and BESS are costly devices. Hence, their appropriate sizing and operational approach are crucial. Yet, the existing works lack the analytical determination of the sizes of these storage devices in perspective of frequency response adequacy. In addition, very few existing works emphasize simultaneously on value proposition of their proposed technique and demonstrating the competency of their adopted methodology with existing frequency response enhancement techniques.

To address these unexplored research gaps, the following contributions are made in this paper.

- Analytical expressions are developed to determine the minimum ratings of SMES and BESS to ensure satisfactory frequency response. To this end, SMES rating is determined using ROCOF limit only due to its dominant participation during inertial response. In addition, BESS rating is decided solely by the allowable frequency deviation due its prominent participation during primary frequency response.
- A strategy is proposed for coordinated operation of SMES and BESS. In this approach, SMES is activated when ROCOF exceeds a certain threshold to provide supplementary inertia. In contrast, BESS is enabled when the frequency deviation crosses a specified limit to provide supplementary inertia and primary frequency support.
- To explore the effectiveness of the proposed methodology, it is applied to a low inertia test power system. Further, the performances of the proposed methodology are compared to that of two existing techniques under various wind penetration cases.
- By analyzing value proposition, it is demonstrated that proposed strategy is more cost effective than an existing solution.

Outcomes of this paper will be helpful for power utilities to enhance the frequency response of low inertia grids. The remaining portions of this paper are structured as follows. Section II describes the grid frequency response characteristics and Energy Storage Systems (ESS) modeling. Then, section III presents the proposed methodology. Next, section IV focuses on the studied power network and simulation scenarios. Further, section V contains simulation results and relevant analyses. Section VI illustrates further discussions and finally, section VII outlines the main findings to conclude the paper.

II. FREQUENCY RESPONSE CHARACTERISTICS AND ESS MODELING

This section provides the basics of inertial response and primary frequency response of a power grid. Later on, modeling approaches of frequency responsive SMES and BESS are articulated.

A. GRID FREQUENCY RESPONSE CHARACTERISTICS

Following an imbalance between load and generation, system frequency exhibits different stages. Just after a contingency, stored kinetic energy from the rotors of synchronous generators is inherently released. This is known as inertial response (IR). Duration of this stage is very low- typically within the first few seconds after a contingency. The next stage is primary frequency response (PFR). In this stage, generators increase their output according to their droop characteristics and headroom (i.e. governor responsive reserve) for stabilizing the system frequency. IR and PFR persist for around 10 – 30 s from the contingency [27]. Quantity and duration of IR and PFR affect the ROCOF (i.e. df/dt) and frequency nadir. Subsequently, secondary frequency response (SFR) comes in action and PFR is relieved. SFR persist for around 15 minutes and can be controlled both automatically and manually. Finally, tertiary frequency response (TFR) brings back the system frequency to its nominal value by re-dispatching the generators. Fig. 1 demonstrates the above-mentioned stages with necessary annotations.

B. FREQUENCY RESPONSE MODELING OF SMES

Electric Power Research Institute (EPRI) CSMEST model is considered in this paper for SMES modeling [28]. Here, SMES is modelled via a Current Source Converter (CSC). AC side of SMES is linked to the grid, whereas the DC side is directly connected to superconducting coil. A general configuration of CSC-based SMES is demonstrated in Fig. 2. Here, the capacitors are deployed for buffering the stored

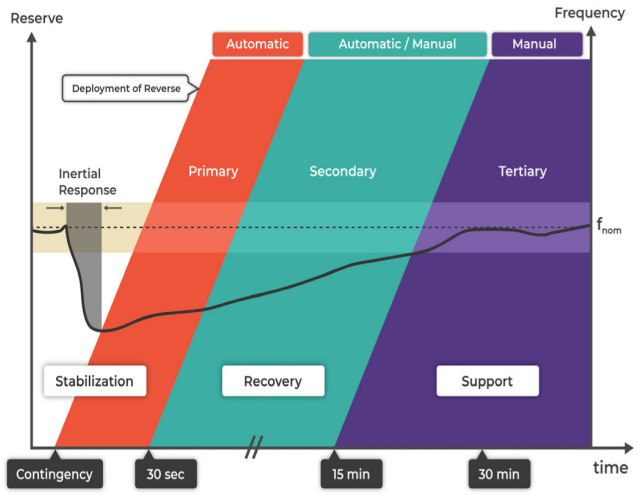

FIGURE 1. Stages of power system frequency response [18].

energy in line inductances while commuting the direction of the grid current. In addition, these capacitors have the capability of filtering out higher order harmonics of the grid current. Fast transfer of active power between SMES and the grid is viable as the modeled SMES in this paper uses CSC. Eventually, it enables SMES to provide emulated inertial response following a contingency.

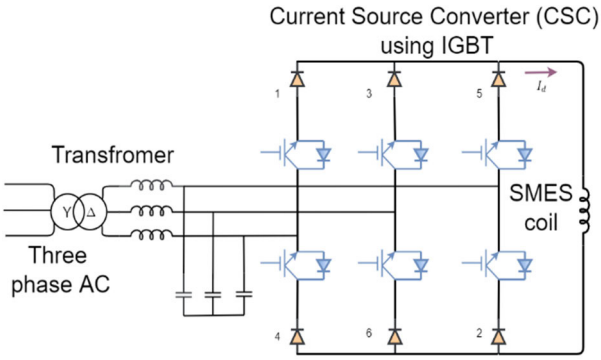

FIGURE 2. General configuration of a CSC-based SMES.

Active power control block of SMES is portrayed in Fig. 3(a). In Fig. 3(a), P_{init} denotes the initial active power of the SMES (in p.u.), I_{DC0} is the initial DC current (in p.u.), I_{DC} refers to the coil DC current (in p.u.), V_{DC} is the coil DC voltage (in p.u.) that depends on coil DC input power P_{DC} (in p.u.), K_R denotes DC current gain and P_{MAX} is the rated power (in p.u.). It is also equal to the minimum current (in p.u.) at which rated power can be delivered (when the maximum DC voltage applied to the coil terminal is 1 p.u.). Maximum voltage capability of the coil and converter is controlled by V_{DCMAX} and V_{DCMIN} (in p.u.) [28]. Note that I_{DC} is an independent variable and V_{DC} is a function of I_{DC}. I_{DCMIN} and I_{DCMAX} are the coil current limits, which prevent the coil overcharging or undercharging. For the upper saturation limit, the value of I_{DC} should be a subset of I_{DCMIN1}. For the lower saturation limit, the chosen value of I_{DC} should be a superset of I_{DCMAX1}.

In this block, converter current limit is modeled by I_{ACMAX} (in p.u.). Lower limit of current coil of CSC is indicated by $KV_{AC}I_{DC}$, where V_{AC} is the grid AC voltage (in p.u.) and K is a constant gain. Also, $MBASE$(in p.u.) is calculated by maximum coil voltage times maximum coil current. The value of SMES coil inductance L (in H) can be derived using power and energy rating of the SMES. Rated energy E_{rated} is calculated using (1) and the corresponding inductance can be derived using (2) [28].

$$E_{rated} = P_{MAX}T \tag{1}$$

$$\frac{1}{2}L\left(I^2 - P_{MAX}^2\right) = P_{MAX}T \tag{2}$$

where T is defined as maximum time duration for delivering power (in s) and I is the maximum coil current (in p.u.).

Input of the active power block is P_{AUX}, which is a ROCOF sensitive auxiliary power signal. This auxiliary signal block is shown in Fig. 3(b). It comprises low pass filter, time delay block, constant gain and max-min limiter block. Therefore, when ROCOF exceeds a preset threshold, this block generates an auxiliary power signal. This auxiliary power signal changes (increase/ decrease) the active power output of SMES. Appropriate values of these parameters are illustrated in Appendix.

C. FREQUENCY RESPONSE MODELING OF BESS

EPRI CBEST model [29] is utilized in this research for BESS modeling. This model uses Voltage-Source Converter (VSC) for grid interfacing. In this topology, grid AC voltage V_{AC} is considered as battery terminal voltage. The amount of power going into and out of the battery is controlled by this voltage. Active power control strategy of BESS is demonstrated in Fig. 4(a). Here P_{AUX}, P_{INIT}, I_{ACMAX} and P_{MAX} indicate the same quantities as of Fig. 3(a).

Fig. 4(b) illustrates the auxiliary power signal model of BESS, where various notations have same meaning as of Fig. 3(b). The auxiliary power signal block of BESS is triggered by frequency deviation. The block generates an auxiliary power signal when frequency deviation exceeds a specified value. Eventually, the active power output of BESS is changed (increase/decrease) via this auxiliary power signal.

The amount of energy absorbed or supplied by the BESS E_{OUT} (in p.u.) depends on input and output efficiencies as shown in Fig. 5. The retrieval efficiency (OUT_{EFF}) is set to be 1.1 and storage efficiency (INP_{EFF}) is chosen to be 0.9 for achieving a turnaround efficiency of 80% [29]. Used values of these parameters are listed in Appendix.

In the next section, analytical expressions are derived to find the minimum ratings SMES and BESS to attain frequency response adequacy. In addition, a strategy is proposed for the prudent deployment of these devices to improve frequency response.

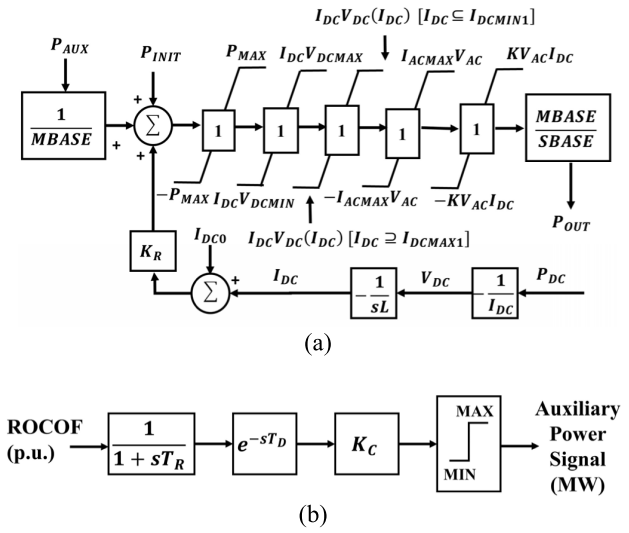

FIGURE 3. (a) Active power control block of CSC-based SMES (b) ROCOF sensitive auxiliary signal model.

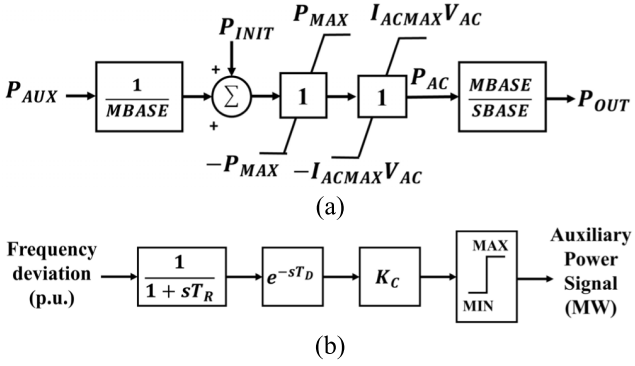

FIGURE 4. (a) Active power control block of BESS (b) Frequency deviation sensitive auxiliary signal model.

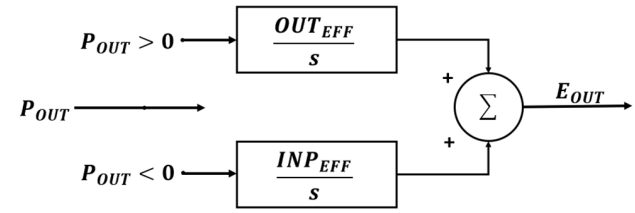

FIGURE 5. Energy control strategy of BESS.

III. PROPOSED METHODOLOGY

In this section, at first, analytical expressions are developed to find the sizes of SMES and BESS to ensure an adequate frequency response. Later on, a methodology is presented for coordinated action of these two ESS.

A. SIZING OF SMES

Since SMES is utilized for short term storage support (i.e. inertial response only), the purpose of utilizing SMES is to restrict the value of ROCOF below the magnitude of maximum allowable limit R_{max} (in Hz/s) after a contingency. This condition can be expressed using (3).

$$ROCOF < R_{max} \tag{3}$$

Note that for a generation loss, ROCOF (df/dt) and maximum allowable ROCOF, both are negative since frequency declines with time. Thus, (3) can be rewritten considering signs of ROCOF and maximum allowable ROCOF.

$$-R_{max} < -ROCOF \tag{4}$$

According to swing equation, following a contingency, ROCOF can be denoted using (5).

$$\frac{df}{dt} = \frac{f_o}{2IR}\left(\Delta P_g - \Delta P_L\right) \tag{5}$$

where f_o is the nominal system frequency (in Hz), IR denotes the system inertia (in MWs), ΔP_g means the change in generation (in MW) and ΔP_L refers to the change in system load (in MW). When n number of synchronous generators are committed, the total inertia IR can be quantified using (6) [30].

$$IR = \sum_{i=1}^{n} (S_i \times H_i) \tag{6}$$

where S_i specifies the rated MVA of i-th synchronous generator and H_i indicates the inertia constant of i-th synchronous generator (in s).

Further, following a loss of generation, ΔP_g can be expressed by (7), where $SMES_{size}$ is the required rated size of SMES (in MW) and g is the contingency size (in MW).

$$\Delta P_g = -g + SMES_{size} \tag{7}$$

Note that SMES is activated to provide inertial response only. Therefore, governor response (refer to Fig. 1) is disregarded in this situation.

In addition, ΔP_L can be written using (8).

$$\Delta P_L = -k_p P_L \left(1 - \frac{f}{f_o}\right) \tag{8}$$

where P_L is the system load including loss (in MW) and k_p is load frequency relief. k_p provides the percentage of load change for every 1% change in system frequency [31]. Using (7) and (8) in (5), the swing equation becomes,

$$\frac{df}{dt} = \frac{f_o}{2IR}\left(k_p P_L \left(1 - \frac{f}{f_o}\right) - g + SMES_{size}\right) \tag{9}$$

Combining (4) and (9),

$$-R_{max} < \frac{f_o}{2IR}\left(k_p P_L \left(1 - \frac{f}{f_o}\right) - g + SMES_{size}\right) \tag{10}$$

By further simplifying, (10) can be rewritten as (11).

$$SMES_{size} > \left[g - \frac{2R_{max}IR}{f_o} - k_p P_L \left(1 - \frac{f}{f_o}\right)\right] \tag{11}$$

Therefore, (11) needs to be satisfied while determining the SMES size for rendering supplementary inertial response.

B. SIZING OF BESS

As stated earlier, BESS can contribute to both IR and PFR following a power imbalance. However, in presence of a SMES, the BESS has relatively higher contribution in the primary frequency response segment compared to inertial response part (demonstrated later in results and discussion section). Accordingly, it is rational to consider frequency deviation thresholds for determining the optimal size of BESS. Thus, the objective of incorporating BESS according to this methodology is to keep the frequency above a predefined threshold f_{min} (in Hz). This condition can be expressed as (12).

$$f > f_{min} \tag{12}$$

where f is instantaneous system frequency (in Hz). When BESS is in action, it can provide primary frequency response along with inertial support. Thus, governor response functionality is also included in ΔP_g. Hence, ΔP_g is modified as shown in (13).

$$\Delta P_g = -g + \sum_{j=1}^{ng} \frac{f_o - f}{R} + BESS_{size} \tag{13}$$

where ng denotes the number of generators with active governors, which can provide primary frequency response according to droop R (in %). $BESS_{size}$ is the required rated size of BESS (in MW) to keep system frequency above a certain value. Using this modified expression of ΔP_g in (4), swing equation can be rewritten as (14).

$$\frac{df}{dt} = \frac{f_o}{2IR}\left[k_p P_L\left(1 - \frac{f}{f_o}\right) - g + BESS_{size} + f_o \sum_{j=1}^{ng} \frac{1}{R}\left(1 - \frac{f}{f_o}\right)\right] \tag{14}$$

For quantifying f, at first, expression of t is obtained by integrating (14).

$$t = -\frac{2IR}{k_p P_L + \left(f_o \sum_{j=1}^{ng} \frac{1}{R}\right)} \ln\left[1 - \left(1 - \frac{f}{f_o}\right) \times \frac{k_p P_L + (f_o \sum_{j=1}^{ng} \frac{1}{R})}{g - BESS_{size}}\right] \tag{15}$$

Further, analytical expression of system frequency f can be obtained by solving (15). It is given by (16).

$$f = f_o\left[1 - \frac{g - BESS_{size}}{(k_p P_L + f_o \sum_{j=1}^{ng} \frac{1}{R})}\left(1 - e^{-\frac{t\left(k_p P_L + f_o \sum_{j=1}^{ng} \frac{1}{R}\right)}{2IR}}\right)\right] \tag{16}$$

In (16), system equivalent time constant T_s can be written by (17).

$$T_s = \frac{2IR}{\left(k_p P_L + f_o \sum_{j=1}^{ng} \frac{1}{R}\right)} \tag{17}$$

Using the expression of T_s in (16), system frequency can be further represented by (18).

$$f = f_o\left[1 - \frac{(g - BESS_{size})T_s}{2IR}\left(1 - e^{-\frac{t}{T_s}}\right)\right] \tag{18}$$

Let, frequency deviation following a contingency is ϕ (in p.u.), which can be expressed by (19).

$$\varphi = \left(1 - \frac{f}{f_o}\right) \tag{19}$$

Combining (18) and (19), frequency deviation is provided by (20).

$$\varphi = -\frac{(g - BESS_{size})T_s}{2IR}\left(e^{-\frac{t}{T_s}} - 1\right) \tag{20}$$

In (20), the lowest value of $e^{-\frac{t}{T_s}}$ can be zero. When $e^{-\frac{t}{T_s}} = 0$, the highest value of frequency deviation after a contingency (φ_{max}) is found. Hence, φ_{max} is expressed via (21).

$$\varphi_{max} = \frac{(g - BESS_{size})T_s}{2IR} \tag{21}$$

The minimum value of system frequency after a contingency i.e., frequency nadir (in Hz) is thus yielded by (22).

$$f_n = f_o - \varphi_{max} f_o = f_o\left(1 - \frac{(g - BESS_{size})T_s}{2IR}\right) \tag{22}$$

Note that for keeping the system frequency above f_{min}, $f_n > f_{min}$ needs to be satisfied. Accordingly, highest allowable frequency deviation, denoted as φ'_{max} can be expressed using (23).

$$\varphi'_{max} = \left(1 - \frac{f_{min}}{f_o}\right) \tag{23}$$

Thus, for satisfying (12), φ'_{max} must be greater than φ_{max}. It results in,

$$-\phi'_{\max} < \frac{(-g + BESS_{size})\, T_s}{2IR} \tag{24}$$

Further modifying (24), expression of required BESS size can be found as follows.

$$BESS_{size} > \left(g - \frac{2IR\phi'_{\max}}{T_s}\right) \tag{25}$$

Using the expression of T_s in (25), analytical expression of required size of BESS can be derived. It is given by (26).

$$BESS_{size} > \left[g - \phi'_{\max}\left(k_p P_L + f_o \sum_{j=1}^{ng} \frac{1}{R}\right)\right] \tag{26}$$

Therefore, (26) has to be satisfied while evaluating the BESS size for catering the desirable primary frequency response.

C. ESS SCHEDULING AND ENERGY RATING

For scheduling the abovementioned ESS (i.e., SMES and BESS) in a power grid, certain constraints need to be satisfied. At first, State of Charge (SoC) values of these ESS are kept within a minimum and maximum range as shown in (27). This prevents the ESS to drain out completely. Violation of this safety limit can impact their lifetime and efficiency.

$$SoC_{min} \leq SoC_t \leq SoC_{max} \forall t \tag{27}$$

where SoC_{min} and SoC_{max} are the minimum and maximum SoC limits respectively. Also, SoC_t is the SoC at any instant, which is defined by (28).

$$SoC_t = SoC_0 - \frac{1}{Q_c} \int I_{DC} dt \tag{28}$$

where SoC_0 refers to initial State of Charge, Q_c is amount charge (in C).

Next, ESS charging and discharging bounds need to be maintained. These conditions are given by (29)-(32) [32].

$$0 \leq P^{ch}_{BESS,t} \leq P^{chmax}_{BESS} \ \forall t \tag{29}$$

$$0 \leq P^{ch}_{SMES,t} \leq P^{chmax}_{SMES} \ \forall t \tag{30}$$

$$0 \leq P^{dch}_{BESS,t} \leq P^{dchmax}_{BESS} \ \forall t \tag{31}$$

$$0 \leq P^{dch}_{SMES,t} \leq P^{dchmax}_{SMES} \ \forall t \tag{32}$$

where $P^{ch}_{BESS,t}$ and $P^{dch}_{BESS,t}$ are the instantaneous amount of charge and discharge of BESS, $P^{ch}_{SMES,t}$ and $P^{dch}_{SMES,t}$ are the instantaneous amount of charge and discharge of SMES. Further, P^{chmax}_{BESS} and P^{chmax}_{SMES} denote the charging limits of BESS and SMES respectively. In addition, P^{dchmax}_{BESS} and P^{dchmax}_{SMES} refer to the discharging limits of BESS and SMES respectively.

By integrating the area under the power curve between ESS triggering instance and the first zero crossing, the amount of energy delivered by ESS can be obtained. Considering 10% tolerance margin and taking retrieval efficiency and storage efficiency into account, energy rating of an ESS can be expressed by (33).

$$E_{ESS} = [\int_{t1}^{t2} P_{out}(t)\, dt OUT_{EFF} + \int_{t1}^{t2} P_{out}(t)\, dt \frac{1}{INP_{EFF}}] 1.1 ESS_{size} \tag{33}$$

where $t1$ is the triggering instance (in s), $t2$ is the first zero crossing instance (in s), E_{ESS} is the energy rating of ESS (in J), P_{out} is the active power output of ESS (in p.u.) and ESS_{size} is the rated size of ESS (in MW). Note that both SMES and BESS are designed to provide 90% of the respective full capacities as the maximum output.

D. PROPOSED STRATEGY FOR COORDINATED ACTION OF ESS

In this subsection, a strategy is proposed for coordinated operation of SMES and BESS. In this scheme, SMES is activated by ROCOF and BESS is triggered by frequency deviation. A system operator can select the appropriate thresholds of ROCOF and frequency deviation based on system requirement.

The main objective of utilizing SMES is to preserve ROCOF within the maximum acceptable value R_{max}. Thus, SMES needs to be triggered before ROCOF reaches R_{max}. In addition, the target behind deploying BESS is to maintain system frequency above a certain threshold f_{min}. As such, the triggering frequency deviation of BESS, ϕ_t has to be less than the maximum allowable frequency deviation φ'_{max}.

The proposed algorithm for coordinated operation of SMES and BESS consists of multiple steps. For ease of understanding, the algorithm is depicted in Fig. 6. The steps are described as follows.

Step-1: Model a low inertia power system having significant renewable penetration.

Step-2: Apply a considerably large contingency such as an interconnection trip or loss of a major generator.

Step-3: For a specific load scenario, via unit commitment scheduling, obtain the generation profile. Use this generation profile to calculate inertia using (6).

Step-4: Using this inertia value, calculate *ROCOF* via (5) for the applied contingency.

Step-5: Check if *ROCOF* exceeds the SMES triggering threshold R_t, where $R_t < R_{max}$. If yes, activate the SMES. If no, proceed to step 6. Note that *ROCOF*, R_t and R_{max} all denote magnitudes of corresponding rate of change of frequency.

Step-6: Calculate system frequency f using (18). Use $\text{BESS}_{\text{size}} = 0$ MW while calculating f. Note that this is the system frequency before including BESS.

Step-7: Calculate frequency deviation ϕ (in p.u.) using (19).

Step-8: Check if ϕ exceeds the BESS triggering frequency deviation ϕ_t (in p.u), where $\phi_t < \varphi'_{max}$. If yes, activate BESS. Otherwise, conclude the process.

Note that this algorithm will be used by the transmission System Operator (TSO) to activate the ESS in case of a contingency. The values of frequency deviation and ROCOF thresholds are also under the jurisdiction of concerned TSO as these thresholds can vary depending on systems requirements, grid codes and energy policies of respective power systems.

To validate the competency of the proposed methodology, it entails to be verified through simulations. To this end, in the next section, the effectiveness of the proposed methodology is explored by applying it to the 59-bus South-East Australian power system.

IV. STUDIED POWER GRID AND SIMULATION SCENARIOS

A. STUDIED POWER SYSTEM

The effectiveness of the proposed methodology is examined in a 50-Hz, 59 bus test network shown in Fig. 7. This network is formed according to the South-East Australian 14-Generator Model [33]. Area-5 in Fig. 7 depicts the low

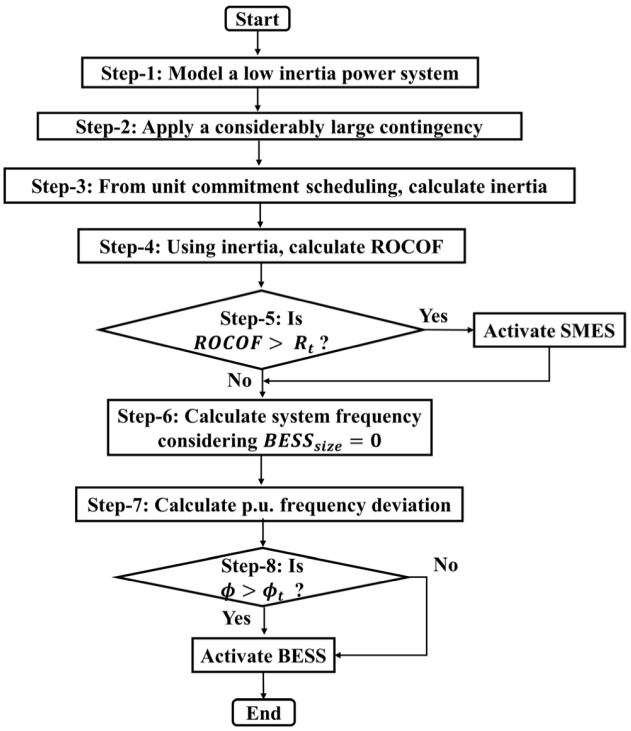

FIGURE 6. Proposed strategy for coordinated operation of SMES and BESS.

inertia grid, which virtually represents the equivalent high voltage transmission network of South Australia.

The number of conventional power plants has significantly reduced in South Australia due to substantial wind power penetration. Consequently, it can be treated as a classic case of a low inertia grid. A 275 kV HVAC interconnection links Area-5 with its adjacent network Area-3 (referred to Victoria).

Two conventional power plants are present in Area-5. These are called TPS_5 and PPS_5, which have multiple generating units. All the generating units have active governors. Table 1 outlines the necessary data of the conventional power plants. Dynamic parameters of these generators are illustrated in the Appendix.

TABLE 1. Conventional powerplant information.

Power plant name	No. of units	Unit capacity (MW)	Unit MVA rating	Unit inertia constant (s)
TPS_5	4	250	333.0	4.0
PPS_5	6	125	166.6	7.5

1) CONVENTIONAL POWERPLANT INFORMATION

The total installed wind generation capacity of Area-5 is assumed to be 1800 MW [34]. In the simulation network, wind power plants are placed at two locations – bus 508 and bus 509 to preserve similarity with the actual geographical positions of South Australian wind power plants. Wind power plants are modelled using type III (DFIG) machines. In addition, SMES and BESS are connected to bus 501. All the dynamic simulations are performed using PSS®E software [35]. This software is extensively used all over the world to study the dynamic responses of power systems. The simulations are carried out using a computer with the following specifications: Intel®core™ i5-8250 CPU@ 1.7-3.4 GHz.

B. SIMULATION SCENARIOS

To take into account various operating conditions, four different scenarios are investigated (denoted by Case study-I to Case study-IV). During low load situation, a few synchronous generators are usually committed. Therefore, the frequency response deteriorates following a disturbance. As such, the total load in Area-5 is presumed to be 1450 MW in all simulation cases to represent a typical low load condition.

During simulation, it is assumed that Area-5 imports power from Area-3 via the interconnection. Frequency response of Area-5 is investigated following the interconnection trip. The number of committed synchronous generators in Area-5 is assumed to be 4 and 3 in various cases. In addition, power import through the interconnection is separately considered as 200 MW and 300 MW. Also, wind generation is varied to simulate different wind penetration levels. The simulation scenarios are outlined in Table 2.

TABLE 2. Simulation scenarios.

Case study	No. of online synchronous generators	Synchronous generation (MW)	Wind generation (MW)	Inertia (MWs)	Interconnection import (MW)
I	4	679	625	5168	200
II	3	450	875	3834	200
III	4	679	525	5168	300
IV	3	450	775	3834	300

1) SIMULATION SCENARIOS

In addition, frequency response performances after adopting the proposed methodology are compared to that of two existing approach: Synchronous Condenser (SC) and "Only BESS". For both of these systems, their rating is considered to be equal to the combined rating of SMES and BESS. Case studies I–IV are analyzed in three separate conditions, viz. without ESS, with ESS and with SC. For comparison purpose, it is assumed that the rating of SC is equal to the cumulative ratings of SMES and BESS. Simulation results and analyses are presented in the next section.

V. RESULTS AND ANALYSES

A. ESS RATINGS

Using the proposed methodology, the ratings of SMES and BESS can be evaluated for any case studies. However, to keep the ratings reasonable yet worthwhile for low inertia situation, case study-II is considered as a baseline. Thus, the required SMES and BESS sizes are determined

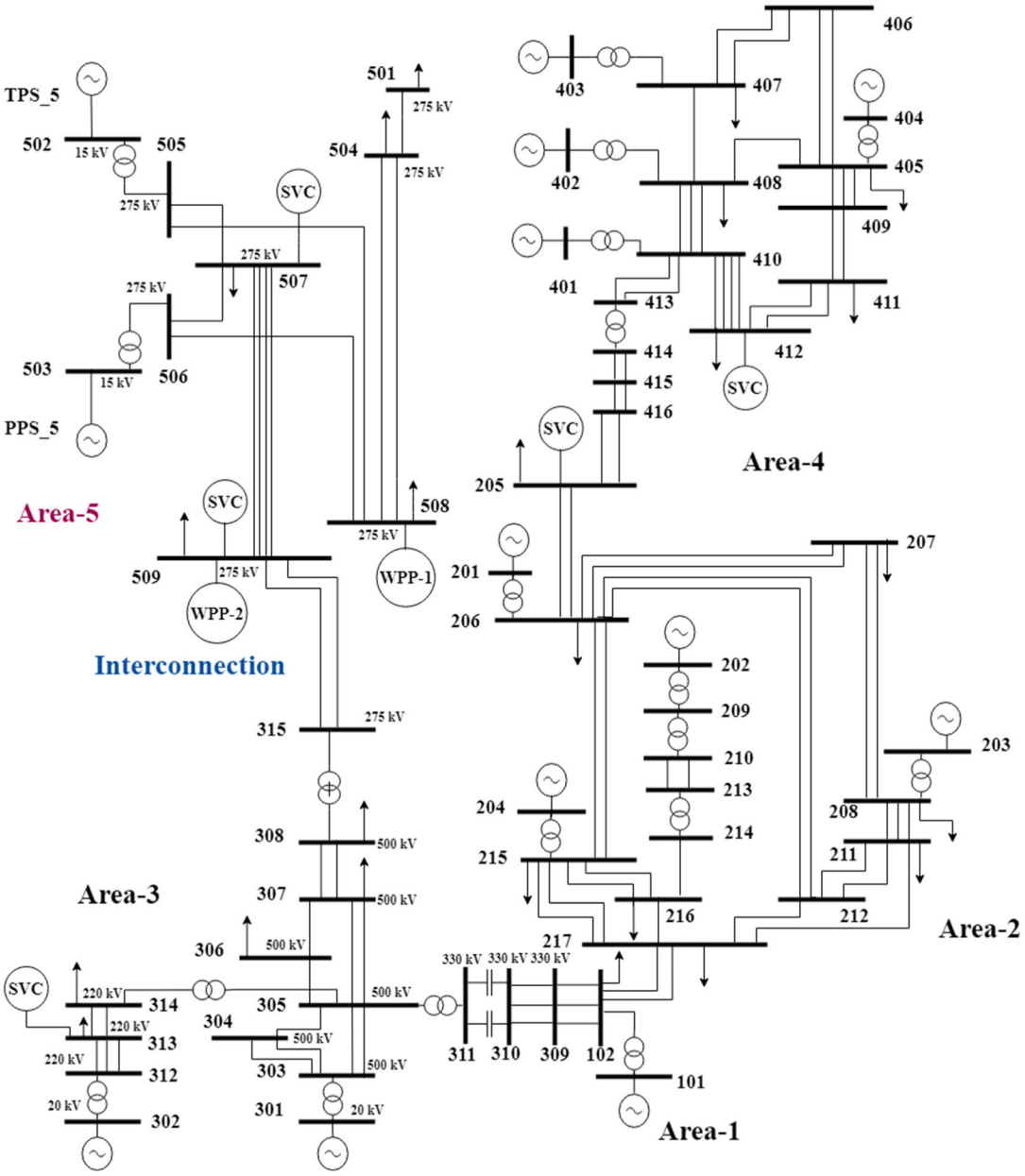

FIGURE 7. Single-line diagram of simulated power system.

considering 3 online synchronous machines while the contingency size is 200 MW. Later on, the frequency response performances are analyzed after incorporating the estimated ESS.

(1) SMES Size: The required SMES size can be determined from (11). The magnitude of maximum allowable ROCOF R_{max} is considered to be 1 Hz/s [36]. In case study-II, $IR = 3834$ MWs, $g = 200$ MW, $k_p = 1.5\%P_L = 1450MW$ and $f_o = 50$ Hz. Hence, by using these values in (11), the minimum SMES rating is found to be around 47 MW.

(2) BESS Size: The required BESS size can be determined from (26). The maximum allowable frequency deviation is assumed to be 1 Hz [37]. Subsequently, ϕ'_{max} is 0.02 p.u. using the base frequency of 50 Hz.

BESS size is also determined for case study-II. Thus, by using $g = 200$ MW, $f_o = 50$ Hz, $R = 5\%$, $k_p = 1.5\%$ and $P_L = 1450$ in (26), the minimum BESS rating is around 97 MW.

Based on the above ratings of SMES and BESS, the SC rating is found to be 144 MVA. Thus, a 144 MVA SC is assumed to be connected to the grid for frequency response comparison. Similarly, for ''only BES'' system, the rating of the BESS is considered to be 144 MW.

B. IMPROVEMENT OF FREQUENCY RESPONSE

Following the contingency, frequencies of online generators are noted. Then, center of frequency (f) is determined using (32) to eliminate small variation in frequencies

of different generators.

$$f = \frac{\sum_{i=1}^{i=n} (f_i \times S_i \times H_i)}{\sum_{i=1}^{i=n} (S_i \times H_i)} \tag{34}$$

where f_i is the frequency of i-th synchronous generator (in Hz).

For all case studies, it is assumed that SMES (rated capacity: 47 MW) is activated when ROCOF after the contingency exceeds 0.5 Hz/s. Further, BESS (rated capacity: 97 MW) is activated when the frequency goes below 49.9 Hz, i.e., frequency deviation exceeds 0.1 Hz (i.e., 0.002 p.u.).

When frequency falls below a certain threshold, the UFLS mechanism is triggered. In this work, it is assumed that the UFLS scheme consists of three stages. The corresponding activation frequencies of these stages are 49 Hz, 48.75 Hz and 48.5 Hz. Also, the UFLS scheme is set to shed 5%, 10% and 15% of the total load at the 1st, 2nd and 3rd stages respectively. Frequency response performances in various case studies are presented as follows.

1) CASE STUDY-I

In this case study, 4 synchronous machines are online and the interconnection is tripped while importing 200 MW power from Area-3. The frequency response curve is shown in Fig. 8(a). Following this contingency, ROCOF is quantified to be 0.96 Hz/s. Hence, ROCOF crosses the 0.5 Hz/s threshold and SMES with a rated capacity of 47 MW is activated. SMES output power is depicted in Fig. 8(b), which necessarily represents an emulated inertial response.

Frequency nadir is 48.98 Hz (without ESS) as depicted by the red trace in Fig. 8 (a). Thus, the frequency deviation is 0.0204 p.u., which surpasses the activation threshold of BESS. Consequently, BESS with a rated capacity of 97 MW is activated as shown in Fig 8(c). It is seen that the BESS output power increases at first when frequency declines. Afterwards, BESS output decreases slowly due to increase in frequency after the nadir point. Fig. 8(c) also justifies the sizing of BESS by considering its PFR contribution. It can be seen that BESS provides around 63 MW active power during IR and 91 MW during PFR when a SMES is also online. Note that a BESS of 97 MW capacity can certainly deliver 63 MW power but not vice-versa.

As UFLS initiates at 49 Hz, system encounters load shedding before utilizing SMES and BESS. The amount of load shedding is 73 MW without ESS. After incorporating both ESS, ROCOF becomes 0.50 Hz/s and frequency nadir becomes 49.61 Hz. Thus, the ROCOF stays below the allowable limit of 1 Hz/s. Furthermore, the frequency excursion stops well above 49 Hz. Consequently, load shedding can be fully avoided after deploying the ESS.

If a synchronous condenser is incorporated instead of ESS, the ROCOF becomes 0.87 Hz/s due to inertial support from SC. However, frequency nadir still stays below 49 Hz (depicted by the blue trace) and system encounters 73 MW load cut. Thus, frequency response significantly improves when the proposed strategy is implemented.

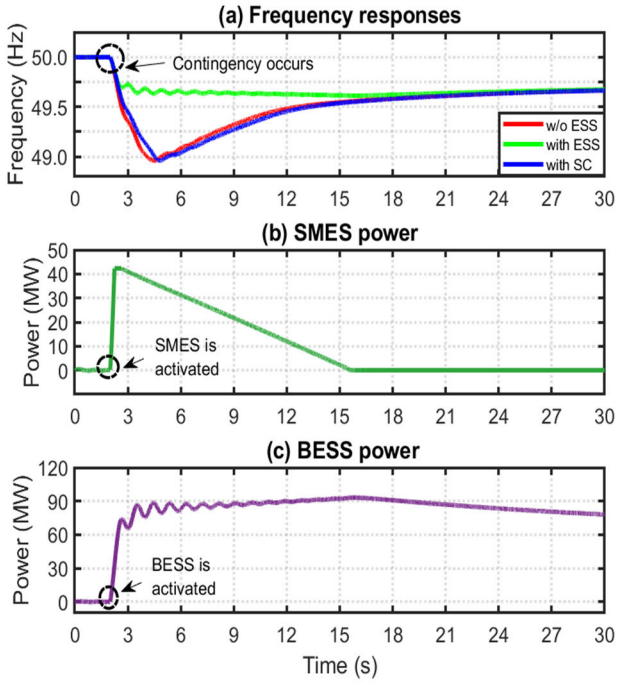

FIGURE 8. (a) Frequency response in case study-I. (b) SMES output in case study-I (c) BESS output in case study-I.

2) CASE STUDY-II

In this case, 200 MW interconnection trip is applied as a contingency while 3 machines are online. For this contingency, ROCOF becomes 1.29 Hz/s. Thereby, ROCOF exceeds the SMES triggering threshold of 0.5 Hz/s. Accordingly, SMES gets activated.

In addition, the frequency nadir without ESS is 48.82 Hz as shown by the red line in Fig. 9(a). Hence, frequency deviation is 0.0236 p.u., which is more than the BESS activation threshold. As a result, BESS is enabled. Consequently, frequency response improves as depicted by the green trace in Fig. 9(a), and frequency nadir becomes 49.50 Hz. Also, ROCOF is found to be 0.57 Hz/s, which stays below the safety limit. The SMES output power is shown in Fig. 9(b) and BESS output power is illustrated in Fig. 9(c).

Note that before activating ESS, frequency falls below 49 Hz. As a result, system incurs 73 MW load shedding. However, frequency excursion stops above 49 Hz after including ESS. Consequently, load shedding is completely averted. When SC is connected instead of ESS, ROCOF is found to be 1.13 Hz/s and frequency nadir is found to be 48.85 as depicted by the blue trace in Fig. 9(a). Hence, neither the ROCOF stays above the 1 Hz/s safety limit nor UFLS is averted. Therefore, Unlike ESS, inclusion of SC does not provide satisfactory frequency response performance. In other words, the proposed method outperforms the existing approach.

3) CASE STUDY-III

In this case, the number of committed synchronous machines is 4 and 300 MW interconnection trip is applied as a

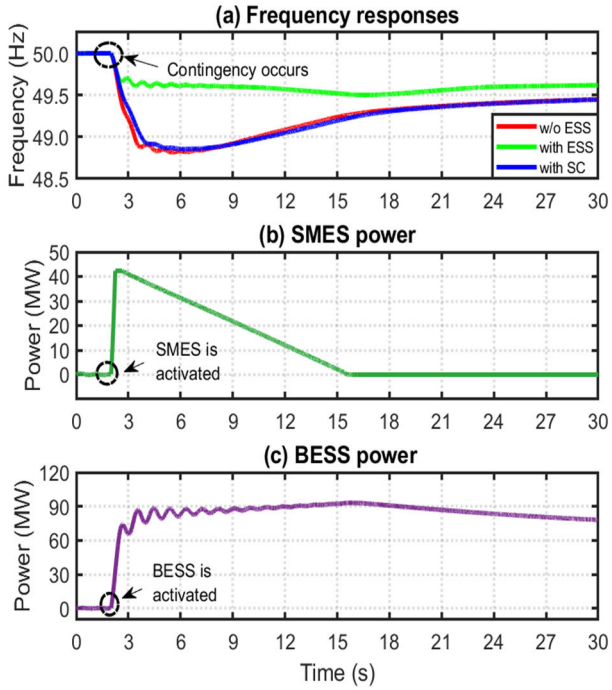

FIGURE 9. (a) Frequency response in case study-II (b) SMES output in case study-II (c) BESS output in case study-II.

contingency. After the loss of interconnection, ROCOF becomes 1.44 Hz/s. In addition, frequency nadir is 48.68 Hz (red line in Fig. 10) when no ESS is incorporated. Thus, the frequency deviation is 1.32 Hz (0.0264 p.u.). As both ROCOF and frequency deviation exceed the respective triggering thresholds, SMES and BESS are activated. After enabling both ESS, ROCOF is quantified to be 0.81 Hz/s. Thus, ROCOF is confined to the maximum limit. In addition, the frequency nadir becomes 48.98 Hz as illustrated by the green trace in Fig. 10. SMES and BESS outputs have the same shapes as of Figs. 9(b) and 9(c).

Before activating ESS, the network experiences 217 MW load shedding. However, it becomes 73 MW when both ESS are enabled. Note that load shedding is not fully stopped because ESS ratings are determined considering 200 MW contingency. Nevertheless, significant reduction in load shedding (144 MW) is achieved when SMES and BESS are instigated. It is to be pointed out that to completely avoid UFLS, ESS sizes needs to be re-estimated for 300 MW contingency. However, ratings would increase in this case, which may cause financial concern for system operators.

Further, when SC is deployed instead of ESS, ROCOF becomes 1.30 Hz/s and frequency nadir becomes 48.73 Hz. Hence, ROCOF exceeds the safety limit and system incurs 217 MW UFLS. Thus, incorporation of SC provides unsatisfactory frequency response.

4) CASE STUDY-IV

In this case, 3 synchronous machines are committed and the contingency size is 300 MW. Following the

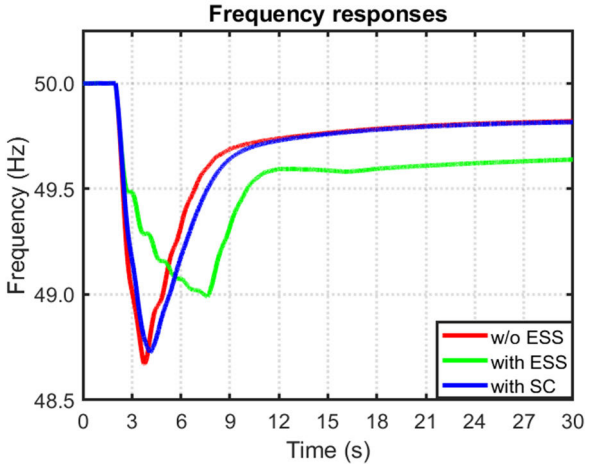

FIGURE 10. Frequency response in case study-III.

interconnection trip, when no ESS is present, ROCOF is found to be 1.94 Hz/s. Also, frequency nadir is 48.63 Hz (which corresponds to 0.0274 p.u. frequency deviation) as depicted by the red line in Fig. 11. Since both ROCOF and frequency deviation surpass respective activation thresholds, both ESS are triggered. Due to supplementary inertia and primary frequency response, frequency excursion improves as shown by the green trace in Fig. 11. It is found that ROCOF reduces to 0.98 Hz/s and the frequency nadir improves to 48.94 Hz after including ESS. Furthermore, load shedding amounts are 217 MW and 73 MW without and with ESS respectively. Therefore, load shedding reduces by 144 MW when SMES and BESS are simultaneously deployed.

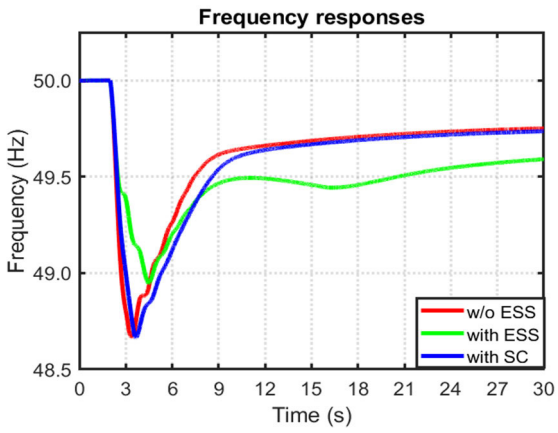

FIGURE 11. Frequency response in case study-IV.

In addition, inclusion of SC as an alternative to ESS yields a ROCOF of 1.70 Hz/s and frequency nadir of 48.64 Hz. As a result, system incurs 217 MW load shedding. Thus, neither ROCOF stays below the safety limit nor UFLS is mitigated by SC incorporation.

C. COMPARISON WITH "ONLY BESS"

In this subsection, the performance of the proposed strategy is compared with "Only BESS" where a BESS of 144 MW capacity is installed instead of the proposed ESS. For the four cases illustrated in Table 2, system frequency response is studied for proposed ESS and "Only BESS".

1) CASE STUDY-I

As stated earlier, in this case study, 4 synchronous machines are online and the interconnection is tripped while importing 200 MW power from Area-3. The frequency response curves for this case are shown in Fig. 12.

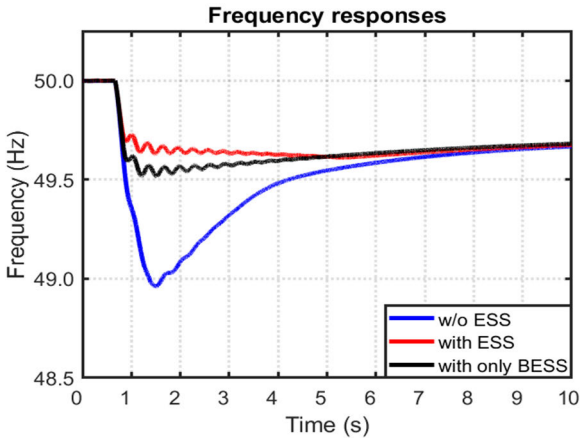

FIGURE 12. Frequency response in case study-I.

The frequency response curves illustrate that following the contingency, with proposed ESS, ROCOF is 0.50 Hz/s and frequency nadir is 49.61 Hz (Red trace). Whereas with an "Only BESS", the ROCOF is found to be 0.52 Hz/s and frequency nadir is found to be 49.51 Hz (Black trace). Thus, the proposed strategy yields slightly better performance than that of "Only BESS".

2) CASE STUDY-II

The frequency response curves for case study-II are portrayed in Fig. 13. The frequency response curves show that following the trip of the 200 MW interconnection, with proposed ESS, ROCOF is 0.57 Hz/s and frequency nadir is 49.50 Hz (Red trace). Nevertheless, with "Only BESS", the ROCOF is found to be 0.58 Hz/s and frequency nadir is found to be 49.48 Hz (Black trace). Thus, the proposed strategy yields almost similar performance compared to that of "Only BESS".

3) CASE STUDY-III

As articulated in the previous subsection, in this case study, 4 synchronous machines are online and the interconnection is tripped while importing 300 MW power from Area-3. The frequency response curves for this case are shown in Fig. 14.

The frequency response curves illustrate that following the contingency, with proposed ESS, ROCOF is 0.81 Hz/s and

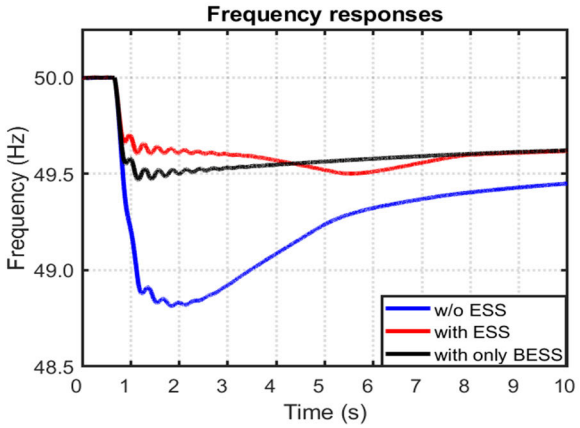

FIGURE 13. Frequency response in case study-II.

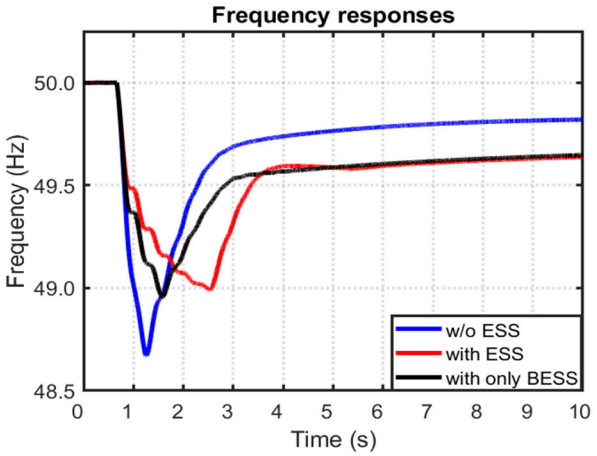

FIGURE 14. Frequency response in case study-III.

frequency nadir is 48.98 Hz (Red trace). When "Only BESS" is considered instead of the proposed strategy, the ROCOF is found to be 0.87 Hz/s and frequency nadir is found to be 48.94 Hz (Black trace). In case of both strategies, 73 MW of load is shed. Thus, again the proposed strategy yields a slightly better system response than that of "Only BESS".

4) CASE STUDY-IV

In this case study, 3 synchronous machines are online and the interconnection is tripped while importing 300 MW power from Area-3 as stated in the earlier subsection. According to the frequency response curves shown in Fig. 15, following the loss of 300 MW power import, with proposed ESS, ROCOF is 0.98 Hz/s and frequency nadir is 48.94 Hz (Red trace). However, if "Only BESS" is incorporated, the ROCOF is found to be 1.02 Hz/s and frequency nadir is found to be 48.92 Hz (Black trace). Note that for "Only BESS", the system ROCOF goes beyond the 1 Hz/s safety limit. Nevertheless, for both strategies, again 73 MW of UFLS is occurred. Therefore, the case studies illustrates that the proposed methodology renders slightly superior system response compared to that of "Only BESS".

TABLE 3. Summary of load simulation results.

Case study	No. of online synchronous generators	Contingency size MW)	ROCOF magnitude (Hz/s)				Frequency nadir (Hz)			
			Without ESS	With SC	With only BESS	With ESS	Without ESS	With SC	With only BESS	With ESS
I	4	200	0.96	0.87	0.52	0.50	48.98	48.99	49.51	49.61
II	3	200	1.29	1.13	0.58	0.57	48.82	48.85	49.48	49.50
III	4	300	1.44	1.30	0.87	0.81	48.68	48.73	48.94	48.98
IV	3	300	1.94	1.70	1.02	0.98	48.63	48.64	48.92	48.94

TABLE 4. Summary of load shedding amounts.

Case study		I	II	III	IV
Load shedding (MW)	Without ESS	73	73	217	217
	With SC	73	73	217	217
	With only BESS	0	0	73	73
	With ESS	0	0	73	73

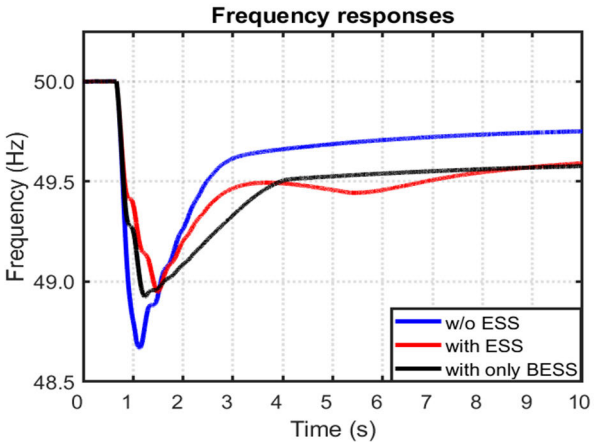

FIGURE 15. Frequency response in case study-IV.

For ease of comparison, simulation results and quantities of load shedding are summarized in Table 3 and Table 4 respectively.

It is evident from the above analyses that the proposed strategy significantly improves the frequency response of the low inertia grid. As such, ROCOF is restricted below the maximum allowable limit and the amount of load shedding considerably reduces when SMES and BESS are activated in a coordinated manner. In addition, the proposed methodology outperforms both SC and "Only BESS" strategy in terms of frequency response adequacy.

D. VALUE PROPOSITION

In this subsection, a value proposition of the proposed methodology (SMES+BESS) is presented. By a comparative cost analysis among SMES+BESS and "Only BESS", this subsection intends to demonstrate that, utilizing a SMES+BESS system is cost effective according to their annual average costs. Here, typical CSC-based SMES and Li-ion BESS are considered. Cost for both systems are threefold: i) Capital cost (C_{cap}) ii) Maintenance cost (C_m) and iii) Operating cost (C_{op}). Mathematical expressions of capital cost and maintenance cost are shown in (35) and (36) respectively [35]. Note that maintenance cost per year is considered as 5% of the capital cost [38].

$$C_{cap} = C_v ESS \tag{35}$$

$$C_m = 0.05 * C_{cap} * ESS * N_{ESS} \tag{36}$$

Here C_v means the capital cost of the specific ESS per MW (in \$/MW), ESS denotes the size of the installed ESS (in MW) and N_{ESS} is the average lifetime of incorporated ESS (in year).

For determining the operational cost of any ESS, it is necessary to consider its energy cycle efficiency and stored energy. Based on these two parameters, average loss can be calculated. Note that energy cycle efficiency of concerned ESS can be defined as (37).

$$\eta = \frac{Stored\ energy}{Stored\ enrgy + Average\ loss} \tag{37}$$

Using the average loss, total annual operating cost can be calculated by (38).

$$C_{op} = Average\ loss * C_{MWh} * N_{ESS} * 365 \tag{38}$$

1) COST ANALYSIS FOR SMES+BESS SYSTEM

For determining the total capital cost or installation cost of the proposed methodology, parameters given in Table 5 are used in (35). It is found that the capital cost of SMES incorporation is 16.45 MUSD and BESS incorporation is 252.2 MUSD. Thus, the total capital cost of the proposed ESS turns out to be $C_{cap} = 268.65$ MUSD.

From the capital costs of SMES and BESS incorporation, their maintenance cost can be calculated using (36). Considering the average lifetimes of SMES and BESS to be 20 year and 12.5 year, their maintenance costs are 16.45 MUSD and 157.65 MUSD respectively. Hence, the total maintenance cost of the proposed ESS is found to be $C_m = 174.1$ MUSD.

For determining the operating cost of the SMES, it is considered that particle detector magnets (solenoid type) are utilized in installed SMES. The stored energy is presumed to be 470MWh (47 MW of the rated output power × 10 hours of the compensation time per day) [38]. Note that the operational cost of SMES includes maintaining cryogenic temperature for the superconducting coil of the SMES. For BESS, a Li-ion battery system is considered, which will store 970 MWh (97 MW of the rated output power × 10 hours of compensation time per day) of energy. Average efficiencies of SMES and BESS are considered to be 98% and 97% respectively [16]. Using these values, the operating cost for SMES is found to be 5.11 MUSD considering its 20 year average lifetime [16]. Similarly, the operating cost for BESS turns out to be 9.99 MUSD considering its 12.5 year average lifetime [16]. Therefore, the total operational cost of the proposed ESS is found to be $C_{op} = 15.1$ MUSD.

The average annual cost can be calculated using (39) when abovementioned three types of costs are known.

$$Average\ annual\ cost = \frac{C_{cap} + C_m + C_{op}}{average\ life\ time\ of\ the\ ESS} \quad (39)$$

Using the values of C_{cap}, C_m, C_{op} and average lifetimes of SMES and BESS, the average annual cost for the proposed methodology is found to be 28.17 MUSD.

TABLE 5. Parameters for cost analysis of proposed ESS [16], [38], [39].

Quantity	Storage type	Value	Unit
C_v	SMES	350000	$/MW
	BESS	2600000	
ESS	SMES	47	MW
	BESS	97	
N_{ESS}	SMES	20	years
	BESS	12.5	
η	SMES	98	percent
	BESS	97	
C_{MWh}	SMES	73	$/MWh
	BESS	73	
$Stored\ energy$	SMES	470	MWh/day
	BESS	970	

2) COST ANALYSIS FOR "ONLY BESS"

For determining the three types of costs for "Only BESS", it is considered that a BESS having 144 MW capacity is installed. Thus, the rating of the BESS is 144 MW in this case. Necessary parameters for cost calculation of this system are given in Table 6.

For determining the total capital cost of "only BES" system, the data illustrated in Table 6 are applied in (35). The total capital cost is found to be 374.4 MUSD in this case. To determine the maintenance cost, the same procedure as the proposed methodology is followed. Using (36), the maintenance cost is found to be 234 MUSD for "Only BESS" considering 12.5 year average lifetime of Li-ion batteries. Afterwards, using (37) and (38), the total operational cost appears to be 14.83 MUSD considering the stored energy to be 1440 MWh (144 MW of the rated output power × 10 hours of compensation time per day).

Using (39), the average annual cost for "Only BESS" is found to be 49.85 MUSD, which results in 76.9% cost increase compared to the proposed methodology. Therefore, if detailed cost analysis is considered, SMES+BESS system offers a cost effective solution than that of "Only BESS".

TABLE 6. Parameters for cost analysis of only BES system [16], [39].

Quantity	Value	Unit
C_v	2600000	$/MW
ESS	144	MW
N_{ESS}	12.5	years
η	97	percent
C_{MWh}	73	$/MWh
$Stored\ energy$	1440	MWh/day

For ease of understanding, all cost components are graphically shown in Fig. 16.

Notably, SMES and BESS cater emulated inertia and primary frequency response for a short duration following a large contingency. The occurrence probabilities of such large contingencies are low. Therefore, it can be assumed that the total operation cost of ESS will not cause any significant financial burden. Considering the above aspects, installation of SMES and BESS can be economically sustainable for low inertia power grids in the long run.

Apart from frequency response adequacy and economic aspect, the proposed strategy yields several further advantages. Also, general applicability of the proposed methodology needs to be articulated. To this end, some additional yet important topics are discussed in the next section.

VI. FURTHER DISCUSSIONS

A. BENEFITS OF THE ANALYTICAL DERIVATIONS

The benefits of the proposed analytical derivations to find the minimum ratings of BESS and SMES are as follows.

- The developed analytical expressions take into account the crucial system parameters such as system frequency deviation, system ROCOF, inertial response and governor response of online synchronous generators for determining minimum ratings of ESS.
- It reduced the dependency on time consuming time-domain simulations and complex optimization algorithms. These algorithms mainly focus on profit maximization instead of power system dynamics while evaluating the ratings of ESS.
- Unlike existing approaches, no linearization of swing equation is done to determine the system frequency. As such, the dynamic attributes of frequency excursion is captured in the proposed analytical derivations.

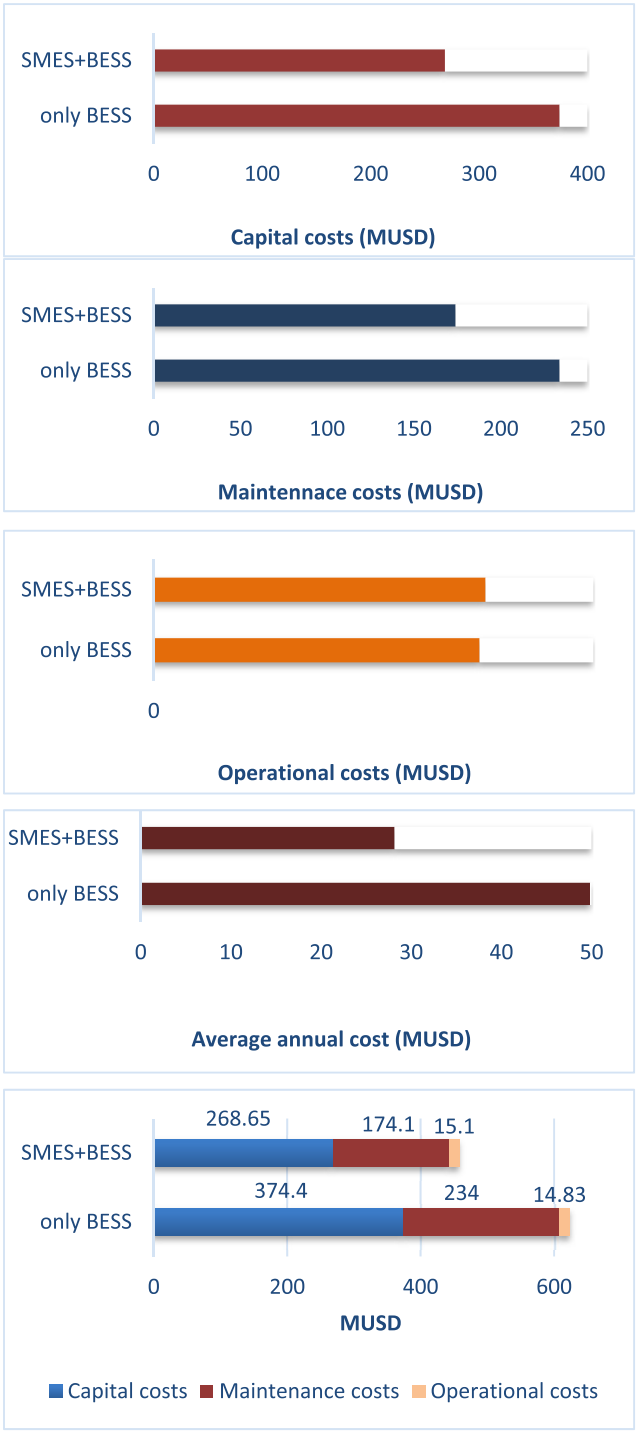

FIGURE 16. Detailed cost analysis of SMES+BESS and "Only BESS."

B. APPLICABILITY OF THE PROPOSED METHOD

It is to be noted that SMES and BESS both have the capacity to charge and discharge at a very rapid rate. In this research work, the ESS is utilized for under-frequency situation where additional active power support is provided by the ESS by discharging rapidly. However, situations can arise where a system is exporting a significant amount of power to its adjacent area and suddenly the interconnection among these two areas trips. As a result, frequency of the power-exporting area can increase and even cross the safety limits [37]. In that case, ESS will be charged to absorb the surplus active power [40]. Thus, the proposed methodology can resolve over frequency issue in renewable dominated grids.

It is to be noted that the proposed methodology will be applied by the TSO during the planning stage to determine the ratings of ESS. According to the grid code, the TSO will choose the threshold values of ROCOF and frequency nadir, which are required for calculating the minimum ratings of the ESS. Afterwards, the ESS can be installed and dispatched accordingly. However, the strategy illustrated in Fig. 6 will be applied by the TSO during operational stage of a power grid. As stated previously, the threshold values for activating SMES and BESS are under the jurisdiction of the concerned TSO. These threshold values can be altered according to the grid requirements. In addition, the thresholds may need to be modified for conforming to the constraints imposed by regulatory bodies.

In this work, variable speed wind turbine generators are considered, which are decoupled from the grid via converters. Therefore, these wind generators usually offer insignificant inertia and governor response when no additional control algorithm is adopted. Likewise, solar photovoltaic (PV) generators are isolated from the network via power electronics interfaces. Hence, a power system under high PV penetration faces similar frequency response challenges as of a wind dominated grid. Therefore, the methodology demonstrated in this paper can also be applied to PV-rich power systems.

C. FACTORS INFLUENCING ESS RESPONSE

It is necessary to ensure that the installed ESS will work properly maintaining its expected response speed. However, few factors can influence the ESS performance and can lead to undesirable response. The following requirements need to be fulfilled for ensuring safe and effective performance of the ESS [41].

The ESS should be able to fulfill the requirements of enhanced frequency response and PFR, which can vary according to the regulation imposed by concerning TSO [42]. By maintaining the SOC management among service windows, according to the National Grid, the ESS should be able to respond within 1 s of the disturbance to provide frequency response [43]. In addition, dedicated ESS for PFR should be able to respond within 10 s of an under-frequency event [43].

- The ESS must be able to deliver or absorb active power thus ensuring delivery in either direction (import to/ export from the host grid).
- The service provider should be able to deliver 100% capacity of the ESS for a minimum of 15 minutes (Supplementary frequency support duration).
- Material quality and cost, energy contents and condition of cell degradation of concerning storages must be analyzed properly.

- The ESS must be able to fulfill its service capability by effectively managing its SoC.

VII. CONCLUSION

In this work, extensive investigations are carried out to explore the roles of SMES and BESS for improving the frequency response of a low inertia grid. To this end, analytical expressions are developed for evaluating the minimum ratings of SMES and BESS. The proposed sizing scheme for ESS has some advantages over its recent counterparts such as reduced dependency on time-domain simulations and time consuming heuristic optimization algorithms and consideration of crucial system operating parameters. Also, a methodology is proposed for coordinated operation of these two ESS. The ratings of SMES and BESS are assessed considering 3 online synchronous machines while the interconnection tripping size is 200 MW. For this contingency, the minimum SMES and BESS ratings are found to be approximately 47 MW and 97 MW respectively to keep ROCOF and frequency deviation within the given acceptable limits.

Frequency response performances are analyzed in four different case studies following the loss of interconnection. Without incorporating ESS (i.e., SMES and BESS), ROCOF is close to or more than 1 Hz/s. Also, the frequency nadirs are less than 49 Hz. Consequently, system encounters significant under-frequency load shedding. In contrast, when ESS are activated, ROCOF is confined to the maximum allowable limit of 1 Hz/s. Furthermore, the frequency nadirs are above 49 Hz (in 200 MW contingency) or very close to 49 Hz (in 300 MW contingency). As a result, load shedding is either fully averted or significantly minimized.

When synchronous condenser (SC) is placed instead of ESS, the ROCOF shows an improving trend due to additional inertial support. However, in three case studies, SC fails to keep ROCOF below the safety threshold. In addition, inclusion of SC does not reduce the amount of load shedding in any case study. When only BESS is incorporated, it yields slightly inferior system performance than that of the proposed methodology. Therefore, it can be revealed that the proposed methodology yields adequate frequency response to make a low inertia grid more secure and resilient. Finally, it is worth stating that the developed technique can be applied to any power system to enhance renewable power penetration by retaining satisfactory frequency response.

APPENDIX

See Tables 7–9.

TABLE 7. Synchronous generator dynamics parameters.

T'_{do}	T''_{do}	T'_{qo}	T''_{qo}	H	D	X_d
7.5	0.04	3.0	0.20	4.0/7.5	0	2.0
X_d	X_q	$X_d{}'$	$X_q{}'$	X''_d	$X_q{}''$	X_l
1.5	0.3	0.8	0.3	0.22	0.22	0.2

TABLE 8. SMES dynamics parameters.

$L, coil\ inductance$	P_{MAX}	V_{DCMAX}	V_{DCMIN}	I_{DCMAX1}
14	0.9	1.0	-1.0	1.0
I_{DCMAX2}	I_{DCMIN1}	I_{DCMIN2}	I_{ACMAX}	K
1.01	0.02	-0.01	1.0	1.0
I_{DCO}	K_R	K_{AVR}	T_1	T_2
0.95	0	0.9	0.01	0.01
T_3	T_4	V_{MAX}	V_{MIN}	Droop
0.01	0.01	9999	-9999	0.01

TABLE 9. Bess dynamics parameters.

P_{MAX}	Out_{Eff}	In_{Eff}	I_{ACMAX}	K_{AVR}	T_1
0.99	1.1	0.9	1.0	1.0	0.01
T_2	T_3	T_4	V_{MAX}	V_{MIN}	Droop
0.01	0.01	0.01	9999	-9999	0.04

REFERENCES

[1] X. Li, Z. Li, L. Guo, J. Zhu, Y. Wang, and C. Wang, "Enhanced dynamic stability control for low-inertia hybrid AC/DC microgrid with distributed energy storage systems," *IEEE Access*, vol. 7, pp. 91234–91242, 2019.
[2] T. Kerdphol, F. S. Rahman, M. Watanabe, Y. Mitani, D. Turschner, and H. P. Beck, "Enhanced virtual inertia control based on derivative technique to emulate simultaneous inertia and damping properties for microgrid frequency regulation," *IEEE Access*, vol. 7, pp. 14422–14433, 2019.
[3] R. Yan, T. K. Saha, N. Modi, N.-A. Masood, and M. Mosadeghy, "The combined effects of high penetration of wind and PV on power system frequency response," *Appl. Energy*, vol. 145, pp. 320–330, May 2015.
[4] H. Gu, R. Yan, T. K. Saha, E. Muljadi, J. Tan, and Y. Zhang, "Zonal inertia constrained generator dispatch considering load frequency relief," *IEEE Trans. Power Syst.*, vol. 35, no. 4, pp. 3065–3077, Jul. 2020.
[5] DNV KEMA Energy & Sustainability. *RoCoF An Independent Analysis on the Ability of Generators to Ride Through Rate of Change of Frequency Values Up to 2 Hz/s*. Accessed: Feb. 10, 2021. [Online]. Available: http://www.eirgridgroup.com/site files/library/EirGrid/DNV_KEMA_Report_RoCoF_20130208final_.pdf
[6] R. Yan, N.-A.-Masood, T. K. Saha, F. Bai, and H. Gu, "The anatomy of the 2016 South Australia blackout: A catastrophic event in a high renewable network," *IEEE Trans. Power Syst.*, vol. 33, no. 5, pp. 5374–5388, Sep. 2018.
[7] S. D. Boeck and D. Van Hertem, "Under frequency load shedding schemes in systems with high PV penetration: Impact and improvements," in *Proc. IEEE Eindhoven PowerTech*, Jun. 2015, pp. 1–6.
[8] N. Masood, R. Yan, T. K. Saha, and S. Bartlett, "Post-retirement utilisation of synchronous generators to enhance security performances in a wind dominated power system," *IET Gener., Transmiss. Distrib.*, vol. 10, no. 13, pp. 3314–3321, Oct. 2016.
[9] H. T. Nguyen, G. Yang, A. H. Nielsen, and P. H. Jensen, "Combination of synchronous condenser and synthetic inertia for frequency stability enhancement in low-inertia systems," *IEEE Trans. Sustain. Energy*, vol. 10, no. 3, pp. 997–1005, Jul. 2018.
[10] X. Zeng, T. Liu, S. Wang, Y. Dong, and Z. Chen, "Comprehensive coordinated control strategy of PMSG-based wind turbine for providing frequency regulation services," *IEEE Access*, vol. 7, pp. 63944–63953, 2019.
[11] I. Sami, N. Ullah, S. M. Muyeen, K. Techato, M. S. Chowdhury, and J.-S. Ro, "Control methods for standalone and grid connected micro-hydro power plants with synthetic inertia frequency support: A comprehensive review," *IEEE Access*, vol. 8, pp. 176313–176329, 2020.
[12] D. Tenfen, E. C. Finardi, B. Delinchant, and F. Wurtz, "Lithium-ion battery modelling for the energy management problem of microgrids," *IET Gener., Transmiss. Distrib.*, vol. 10, no. 3, pp. 576–584, Feb. 2016.
[13] A. Saleh, A. Awad, and W. Ghanem, "Modeling, control, and simulation of a new topology of flywheel energy storage systems in microgrids," *IEEE Access*, vol. 7, pp. 160363–160376, 2019.
[14] R. K. Sarojini and P. Kaliannan, "Inertia emulation through supercapacitor for a weak grid," *IEEE Access*, vol. 9, pp. 30793–30802, 2021.

[15] X. Lin and Y. Lei, "Coordinated control strategies for SMES-battery hybrid energy storage systems," *IEEE Access*, vol. 5, pp. 23452–23465, 2017.
[16] M. Farhadi and O. Mohammed, "Energy storage technologies for high-power applications," *IEEE Trans. Ind. Appl*, vol. 52, no. 3, pp. 1953–1961, May/Jun. 2015.
[17] G. Delille, B. Francois, and G. Malarange, "Dynamic frequency control support by energy storage to reduce the impact of wind and solar generation on isolated power system's inertia," *IEEE Trans. Sustain. Energy*, vol. 3, no. 4, pp. 931–939, Oct. 2012.
[18] A. Oudalov, D. Chartouni, and C. Ohler, "Optimizing a battery energy storage system for primary frequency control," *IEEE Trans. Power Syst.*, vol. 22, no. 3, pp. 1259–1266, Aug. 2007.
[19] H. Xie, X. Teng, Y. Xu, and Y. Wang, "Optimal energy storage sizing for networked microgrids considering reliability and resilience," *IEEE Access*, vol. 7, pp. 86336–86348, 2019.
[20] A. J. Headley and D. A. Copp, "Energy storage sizing for grid compatibility of intermittent renewable resources: A California case study," *Energy*, vol. 198, May 2020, Art. no. 117310.
[21] U. T. Salman, F. S. Al-Ismail, and M. Khalid, "Optimal sizing of battery energy storage for grid-connected and isolated wind-penetrated microgrid," *IEEE Access*, vol. 8, pp. 91129–91138, 2020.
[22] M. Li, L. Wang, Y. Wang, and Z. Chen, "Sizing optimization and energy management strategy for hybrid energy storage system using multiobjective optimization and random forests," *IEEE Trans. Power Electron.*, vol. 36, no. 10, pp. 11421–11430, Oct. 2021.
[23] V. Knap, S. K. Chaudhary, D.-I. Stroe, M. Swierczynski, B.-I. Craciun, and R. Teodorescu, "Sizing of an energy storage system for grid inertial response and primary frequency reserve," *IEEE Trans. Power Syst.*, vol. 31, no. 5, pp. 3447–3456, Sep. 2016.
[24] J. Li, A. M. Gee, M. Zhang, and W. Yuan, "Analysis of battery lifetime extension in a SMES-battery hybrid energy storage system using a novel battery lifetime model," *Energy*, vol. 86, pp. 175–185, Jun. 2015.
[25] T. Ise, M. Kita, and A. Taguchi, "A hybrid energy storage with a SMES and secondary battery," *IEEE Trans. Appl. Supercond.*, vol. 15, no. 2, pp. 1915–1918, Jun. 2005.
[26] J. Li, M. Zhang, Q. Yang, Z. Zhang, and W. Yuan, "SMES/battery hybrid energy storage system for electric buses," *IEEE Trans. Appl. Supercond.*, vol. 26, no. 4, pp. 1–5, Jun. 2016.
[27] J. Van de Vyver, J. D. M. D. Kooning, B. Meersman, L. Vandevelde, and T. L. Vandoorn, "Droop control as an alternative inertial response strategy for the synthetic inertia on wind turbines," *IEEE Trans. Power Syst.*, vol. 31, no. 2, pp. 1129–1138, Mar. 2015.
[28] *PSS E User Manual, Version 34.2, Program Application Guide*, Siemens Ind., Schenectady, NY, USA, 2017, ch. 25, pp. 8–25, vol. 2.
[29] S. Eckroad, "EPRI-DOE handbook of energy storage for transmission & distribution applications," Electr. Power Res. Inst., Washington, DC, USA, Tech. Rep. 000000000001001834, 2003, pp. 349–372.
[30] S. Kumar, R. K. Saket, D. K. Dheer, J. B. Holm-Nielsen, and P. Sanjeevikumar, "Reliability enhancement of electrical power system including impacts of renewable energy sources: A comprehensive review," *IET Gener., Transmiss. Distrib.*, vol. 14, no. 10, pp. 1799–1815, May 2020.
[31] N. A. Masood, R. Yan, and T. K. Saha, "Investigation of load frequency relief from field measurements and its impact on contingency reserve evaluation," *IEEE Trans. Power Syst.*, vol. 33, no. 1, pp. 567–577, May 2017.
[32] P. Kushwaha, V. Prakash, R. Bhakar, U. R. Yaragatti, Y. Sumanth, and A. Jain, "Primary frequency response constrained energy storage scheduling under photovoltaic generation," in *Proc. 8th Int. Conf. Power Syst. (ICPS)*, Dec. 2019, pp. 1–5.
[33] M. Gibbard and D. Vowles, "Simplified 14-generator model of the SE Australian power system," Revision 3, Univ. Adelaide, Adelaide, SA, Australia, Tech. Rep. 3, Jun. 2010.
[34] RenewablesSA. *Government of South Australia*. Accessed: Jun. 9, 2020. [Online]. Available: http://www.renewablessa.sa.gov.au/topic/large-scale-generation-storage/wind-farms-south-australia
[35] PSS E. *Power System Simulator for Engineering*. Accessed: Mar. 3, 2021. [Online]. Available: http://www.energy.siemens.com/hq/en/services/power-transmission-distribution/power-technologies-international/software-solutions
[36] Australian Energy Market Commission. (2020). *National Electricity Rules*. Version 156, ch. 5, p. 731. Accessed: Jul. 2, 2021. [Online]. Available: https://www.aemc.gov.au/sites/default/files/2020-12/NER%20v156%20full.pdf
[37] Australian Energy Market Commission. (2020). *Frequency Operating Standards*. Accessed: Jul. 2, 2021. [Online]. Available: https://www.aemc.gov.au/australias-energy-market/market-legislation/electricity-guidelines-and-standards/frequency-0
[38] S. Nomura, T. Shintomi, S. Akita, T. Nitta, R. Shimada, and S. Meguro, "Technical and cost evaluation on SMES for electric power compensation," *IEEE Trans. Appl. Supercond.*, vol. 20, no. 3, pp. 1373–1378, Jun. 2010.
[39] *Australian Energy Regulator*. AER. Accessed: Jul. 2, 2021. [Online]. Available: https://www.aer.gov.au/wholesale-markets/wholesale-statistics/annualvolume-weighted-average-spot-prices-regions
[40] N.-A. Masood, M. N. H. Shazon, H. M. Ahmed, and S. R. Deeba, "Mitigation of over-frequency through optimal allocation of BESS in a low-inertia power system," *Energies*, vol. 13, no. 17, p. 4555, Sep. 2020.
[41] D. M. Greenwood, K. Y. Lim, C. Patsios, P. F. Lyons, Y. S. Lim, and P. C. Taylor, "Frequency response services designed for energy storage," *Appl. Energy*, vol. 203, pp. 115–127, Oct. 2017.
[42] National Grid. (2016). *Enhanced Frequency Response*. Accessed: Aug. 10, 2021. [Online]. Available: http://www2.nationalgrid.com/Enhanced-Frequency-Response.aspx
[43] National Grid. (2016). *System Operability Framework*. Accessed: Aug. 11, 2021. [Online]. Available: https://www.nationalgrid.com/sites/default/files/documents/8589937803-SOF%202016%20-%20Full%20Interactive%20Document.pdf

MD. NAHID HAQUE SHAZON (Graduate Student Member, IEEE) received the B.Sc. degree in electrical and electronic engineering (EEE) from Bangladesh University of Engineering and Technology (BUET), Dhaka, Bangladesh, in 2019, where he is currently pursuing the M.Sc. degree in electrical and electronic engineering. He is also working as a Lecturer with the Department of EEE, BRAC University, Dhaka. His research interests include power system analysis, grid integration of renewable energy, power system modeling, and solar cell research.

NAHID-AL-MASOOD (Senior Member, IEEE) received the B.Sc. and M.Sc. degrees in electrical and electronic engineering (EEE) from Bangladesh University of Engineering and Technology (BUET), Dhaka, Bangladesh, in 2008 and 2010, respectively, and the Ph.D. degree in power and energy systems from The University of Queensland, Brisbane, Australia, in 2017. He is currently working as an Associate Professor with the Department of EEE, BUET. His research interests include power system modeling and analysis and grid integration of renewable energy.

HASIN MUSSAYAB AHMED received the B.Sc. degree in electrical and electronic engineering (EEE) from Bangladesh University of Engineering and Technology (BUET), Dhaka, Bangladesh, in 2019, where he is currently pursuing the M.Sc. degree in electrical and electronic engineering. His research interests include power system analysis and renewable energy.

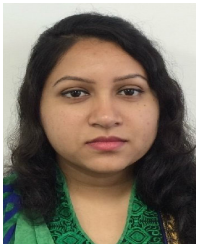

SHOHANA RAHMAN DEEBA (Member, IEEE) received the B.Sc. and M.Sc. degrees in electrical and electronic engineering (EEE) from Bangladesh University of Engineering and Technology (BUET), Dhaka, Bangladesh, in 2009 and 2013, respectively, and the Ph.D. degree in power and energy systems from The University of Queensland, Brisbane, Australia, in 2017. She is currently working as an Assistant Professor with the Department of Electrical and Computer Engineering, North South University, Dhaka. Her research interests include power system modeling, distribution system analysis, and renewable energy integration.

EKLAS HOSSAIN (Senior Member, IEEE) received the B.S. degree in electrical and electronic engineering from Khulna University of Engineering and Technology, Bangladesh, in 2006, the M.S. degree in mechatronics and robotics engineering from International Islamic University Malaysia, Malaysia, in 2010, and the Ph.D. degree from the College of Engineering and Applied Science, University of Wisconsin–Milwaukee (UWM). He has been working in the area of distributed power systems and renewable energy integration for last ten years. He is now involved with several research projects on renewable energy and grid tied microgrid system at Oregon Tech, as an Associate Professor with the Department of Electrical Engineering and Renewable Energy, since 2015. He is currently working as an Associate Researcher with Oregon Renewable Energy Center (OREC). He is also a Registered Professional Engineer (PE) in the State of Oregon, USA. He is also a Certified Energy Manager (CEM) and a Renewable Energy Professional (REP). He has published a number of research papers and posters in this field. His research interests include modeling, analysis, design, and control of power electronic devices, energy storage systems, renewable energy sources, integration of distributed generation systems, microgrid and smart grid applications, robotics, and advanced control systems. He and his dedicated research team, is looking forward to explore methods to make the electric power systems more sustainable, cost-effective and secure through extensive research and analysis on energy storage, microgrid systems, and renewable energy sources. He is a Senior Member of the Association of Energy Engineers (AEE). He is the winner of the Rising Faculty Scholar Award from Oregon Institute of Technology, in 2019, for his outstanding contribution in teaching. He is serving as an Associate Editor for IEEE Access.